Electronic Supplementary Material (ESI) for Journal of Materials Chemistry A.

One-step solid phase synthesis of highly efficient and robust cobalt pentlandite electrocatalyst for oxygen evolution reaction

Mohammad Al-Mamun,[a] Yun Wang,*[a] Porun Liu,[a] Yulin Zhong,[a] Huajie Yin,[a] Xintai Su,[a,b] Haimin Zhang,[c] Huagui Yang,[a] Dan Wang,[a] Zhiyong Tang,[a] Huijun Zhao*[ac]

[a]Centre for Clean Environment and Energy, Griffith University, Gold Coast Campus, QLD 4222, Australia

[b]Ministry Key Laboratory of Oil and Gas Fine Chemicals, College of Chemistry and Chemical Engineering, Xinjiang University, Urumqi 830046, China

[c]Centre for Environmental and Energy Nanomaterials, Institute of Solid State Physics, Chinese Academy of Sciences, Hefei 230031, China

*Corresponding authors. Tel.: +61 7 5552 8261; Fax: +61 7 5552 8067

E-mail addresses: h.zhao@griffith.edu.au (H. Zhao); yun.wang@griffith.edu.au (Y. Wang)

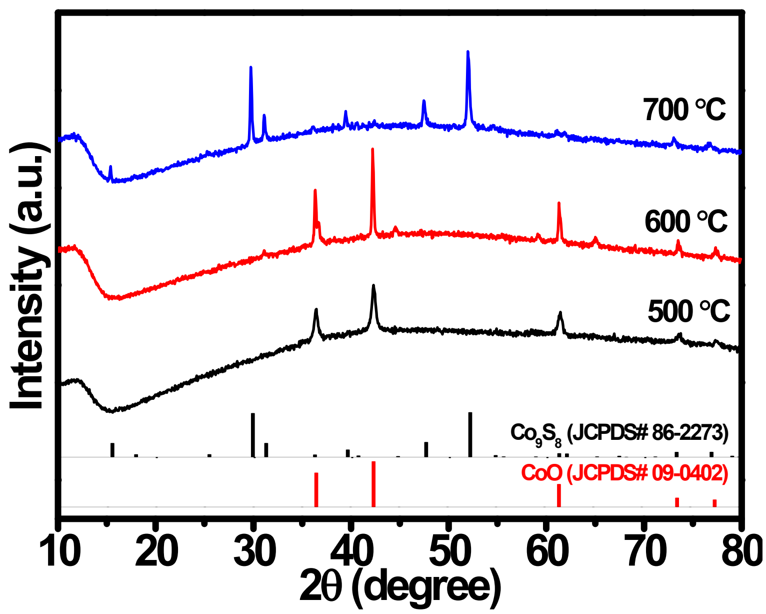

Fig. S1 XRD patterns of the samples prepared at different calcination temperatures (500-700 °C).

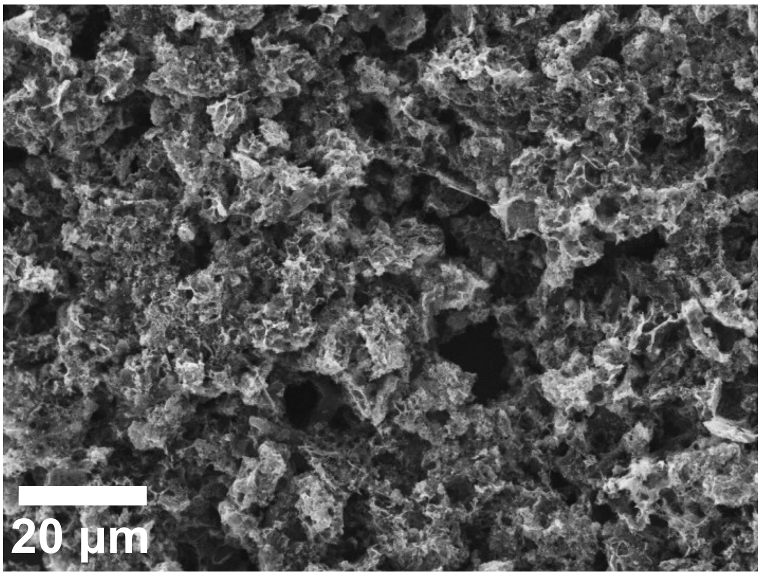

Fig. S2 Low magnification SEM image of Co_9S_8/CNS nanocomposite prepared at 700 °C.

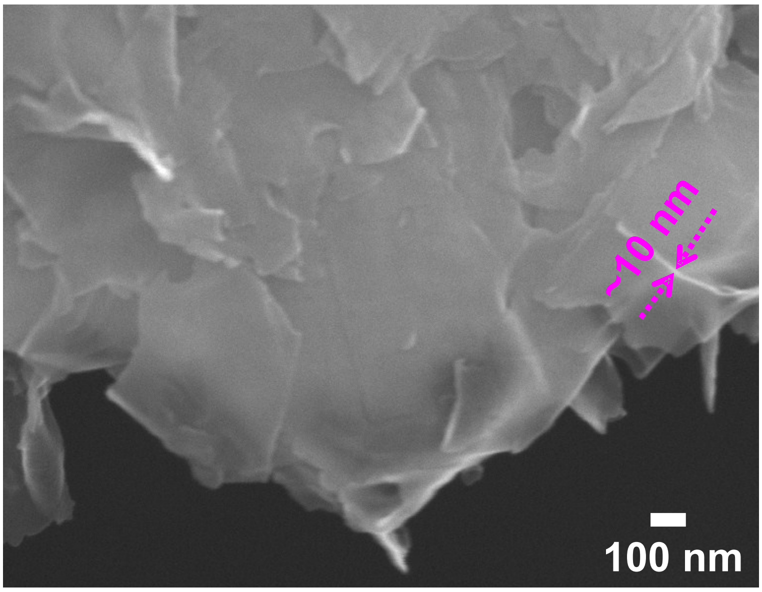

Fig. S3 SEM image of CNS prepared at 700 °C showing the lateral size of several μm with the thickness of ~10 nm.

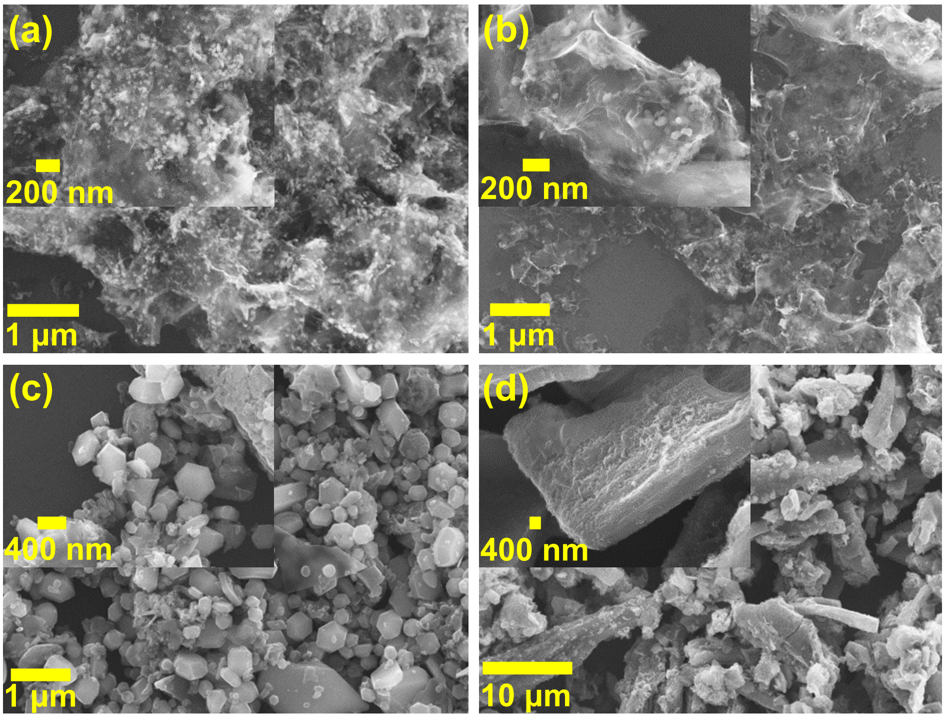

Fig. S4 SEM images of the synthesised samples prepared at calcination temperature of (a) 500, (b) 600, (c) 800 and (d) 900 °C.

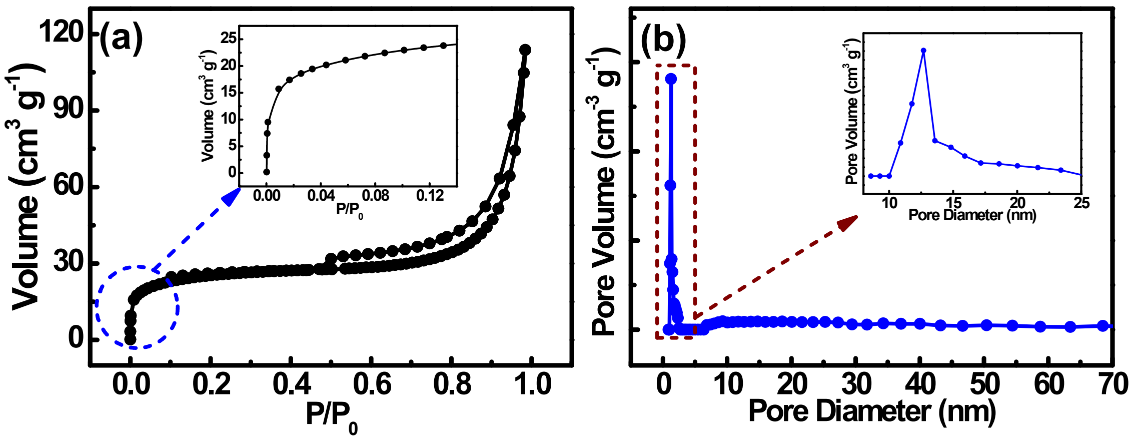

Fig. S5 (a) BET and (b) pore size distribution curves of Co_9S_8/CNS nanocomposite. The insets in (a) and (b) show the enlarged BET curve in low P/P_0 range and the distribution curves of mesopores, respectively.

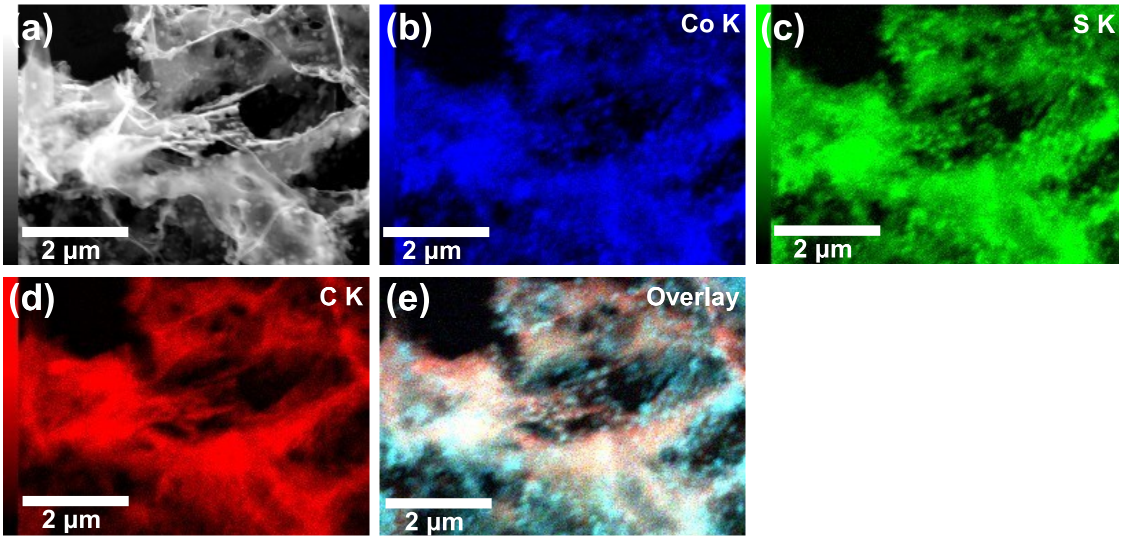

Fig. S6 (a) SEM image, and (b) cobalt, (c) sulfur, (d) carbon and (e) overlay elemental mapping of Co_9S_8/CNS nanocomposite.

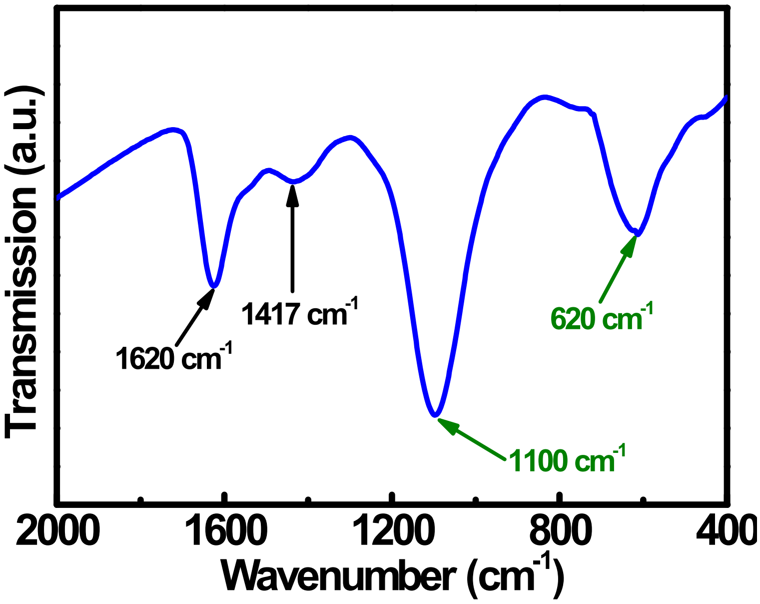

Fig. S7 FTIR spectrum of Co_9S_8/CNS nanocomposite.

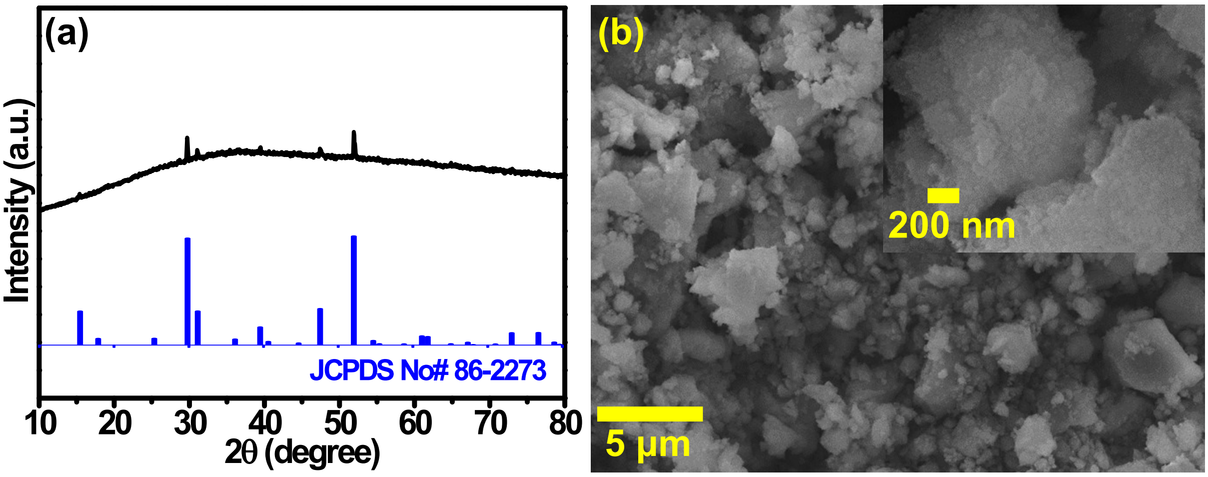

Fig. S8 (a) XRD pattern and (b) SEM images of Co_9S_8 NPs prepared by a hydrothermal method reported elsewhere[1] and calcined at 700 °C under Ar atmosphere.

Table S1. A summary of the OER performances of cobalt based chalcogenide catalysts in 1.0 M KOH electrolyte.[a]

Catalysts	η@10 mA cm^{-2} (mV)	Onset potential (V vs. RHE)	Tafel slope (mV dec^{-1})	Mass loading (mg cm^{-2})	Substrate	Reference
Co_9S_8/CNS/CNT	267	~1.45	48.2	0.24	GCE	This work
Co_9S_8/CNS	294	~1.45	50.7	0.24	GCE	This work
CP/CTs/Co-S	300	~1.50	72.0	0.32	CP	[2]
CoO_x-CoSe/NF	300[(b)]	~1.50	68	1.7	Ni foam	[3]
$Ni_{2.3\%}$-CoS_2	~310	~1.53	119	0.97	CC	[4]
Fe_3O_4@Co_9S_8/rGO	320	1.48	54.5	0.25	GCE	[5]
Co_9S_8@NC	320	~1.40	-	0.22	GCE	[6]
$Co_{0.85}Se$	324	~1.45	85	0.6	Carbon cloth	[7]
$Zn_{0.76}Co_{0.24}S/CoS_2$	~325	~1.54	79	1.0	Ti	[8]
CoS	361	~1.55	64	-	Ti	[9]
$Co_{0.5}Fe_{0.5}S$@N-MC	410	~1.57	159	0.1	GCE	[10]
Co_9S_8@MoS_2/CNFs	430	~1.58	61	0.21	GCE	[11]
$CoSe_2$	430	~1.57	50	1.0	GCE	[12]
Co_9S_8/CNFs	512	~1.62	78	0.21	GCE	[11]

[a]The table is sorted in descending order by η@10 mA cm^{-2}, the overpotential required to reach the current density of 10 mA cm^{-2}; [b]the overpotential @100 mA cm^{-2}.

Table S2. A summary of the OER performances of cobalt based chalcogenide catalysts in 0.1 M KOH electrolyte.[a]

Catalysts	η@10 mA cm^{-2} [mV][(a)]	Onset potential [V vs. RHE]	Tafel slope [mV dec^{-1}]	Mass loading [mg cm^{-2}]	Substrate	Reference
Co_9S_8/CNS/CNT	299	~1.46	59.8	0.24	GCE	This work
Co_9S_8/CNS	324	~1.46	67.9	0.24	GCE	This work
Fe_3O_4@Co_9S_8/rGO	340	1.48	65.5	0.25	GCE	[5]
Co_9S_8/N-C	~347	~1.48	69.0	0.80	GCE	[13]
$Co_{1-x}S$/G	~349	~1.52	55.6	0.0926	GCE	[14]
Co_3S_4	363	~1.52	90	0.283	GCE	[15]
NG-$CoSe_2$	366	~1.50	40	0.20	GCE	[16]
Co_9S_8@NC	370	~1.40	124	0.22	GCE	[6]
CoS_2/N,S-GO	380	~1.50	75	0.25	GCE	[17]
Co_9S_8/G	409	~1.52	82.7	0.20	GCE	[18]
Mn_3O_4/$CoSe_2$	420	~1.48	49	0.20	GCE	[19]
Co_3S_4/NCNTs	430	~1.55	70	0.20	GCE	[20]
$NiCo_2S_4$@N/S-rGO	470	~1.57	-	0.283	GCE	[21]
Co_xS_y@C	470	~1.56	-	0.141	GCE	[22]
$CoSe_2$	510	~1.57	67	1.0	GCE	[12]

[a]The table is sorted in descending order by η@10 mA cm^{-2}.

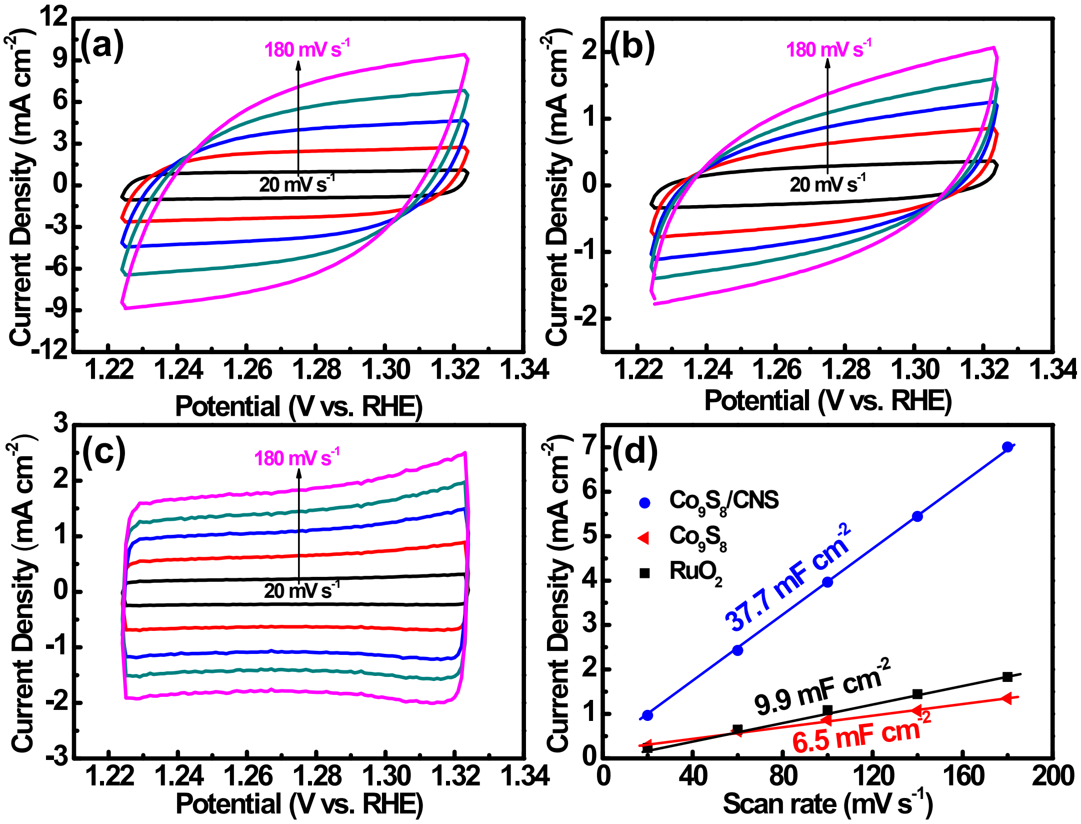

Fig. S9 Cyclic voltammograms at scan rates from 20 to 180 mV s^{-1} under the non-Faradic potential window of 1.224 to 1.324 V (vs. RHE) of (a) Co_9S_8/CNS, (b) Co_9S_8 and (c) RuO_2; (d) Plots of current densities at 1.275 V vs. scan rates of Co_9S_8/CNS, Co_9S_8 and RuO_2, respectively.

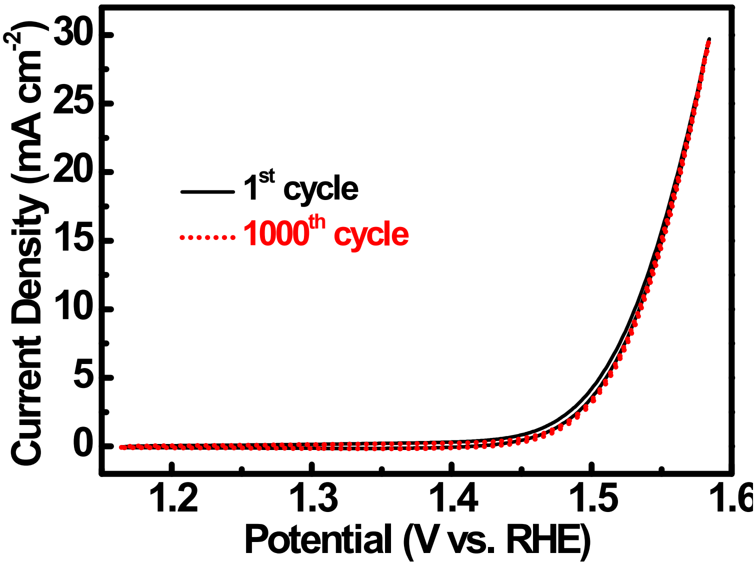

Fig. S10 The first and 1000th CV cycle of Co_9S_8/CNS in 1.0 M KOH electrolyte at a scan rate of 10 mV s^{-1}.

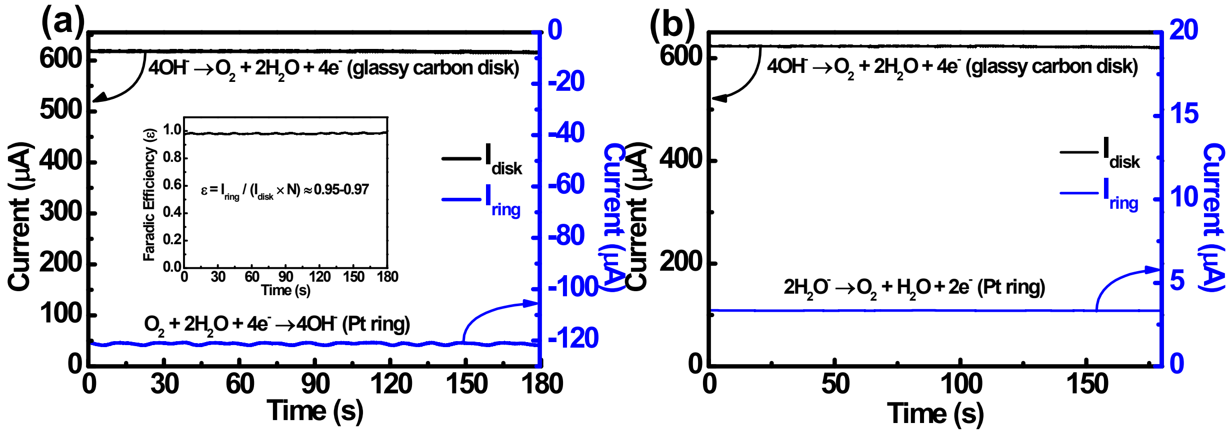

Fig. S11 (a) Disk current (I_{disk}) and ring current (I_{ring}) of Co_9S_8/CNS using RRDE measurements under the applied potential of 1.52 V (vs. RHE) at the disk (GCE) and 0.4 V (vs. RHE) at the ring (Pt); the inset shows the Faradic efficiency of Co_9S_8/CNS for OER; (b) Disk current (I_{disk}) and ring current (I_{ring}) of Co_9S_8/CNS using RRDE measurements for the detection of H_2O_2 generation under the applied potential of 1.52 V (vs. RHE) at the disk (GCE) and 1.5 V (vs. RHE) at the ring (Pt). All the RRDE measurements are conducted in N_2-saturated, 1.0 M KOH electrolyte.

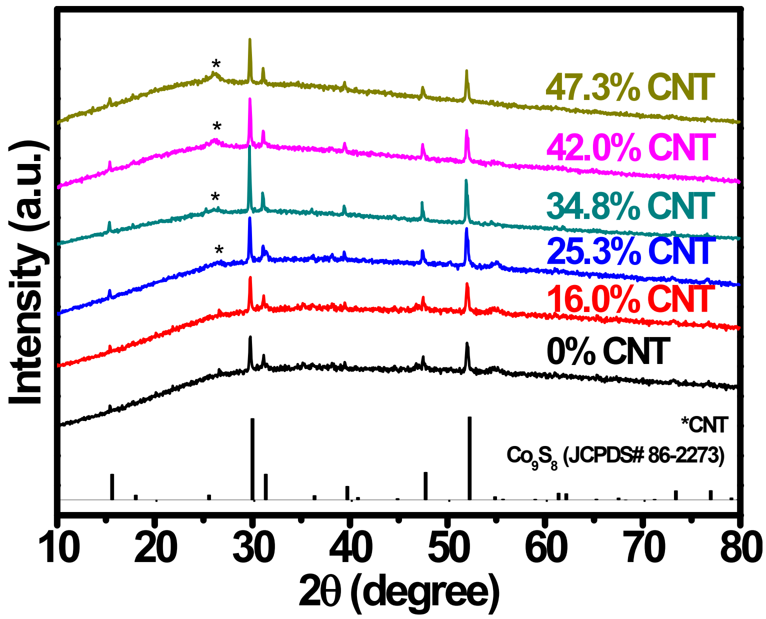

Fig. S12 XRD patterns of the nanocomposites prepared with different contents of CNT. CNT peak is highlighted with "*".

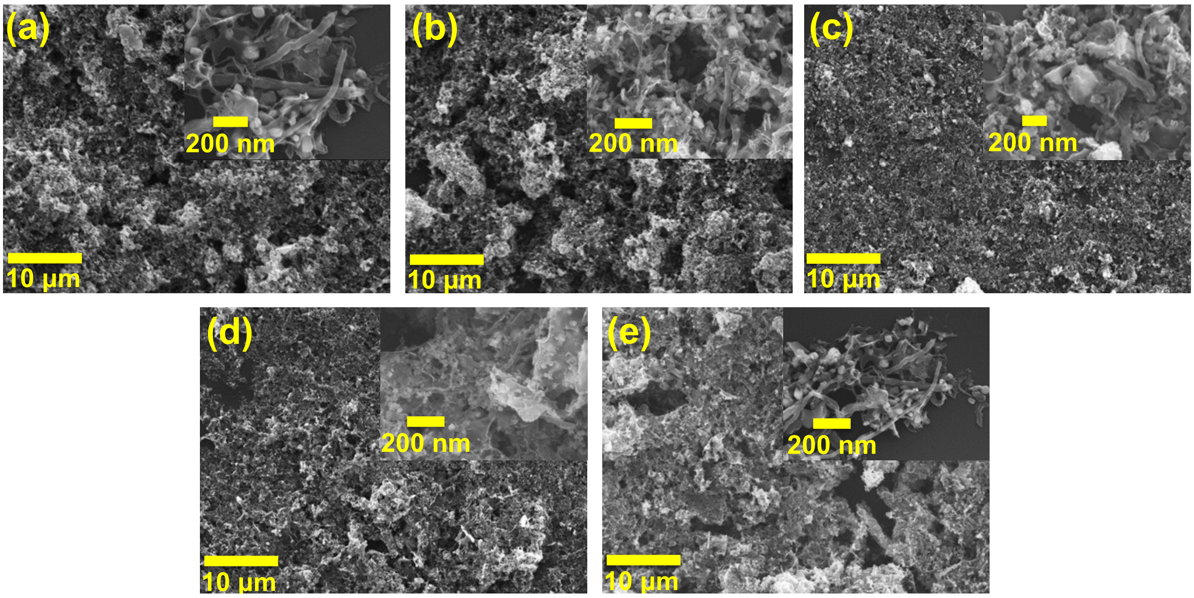

Fig. S13 SEM images of Co_9S_8/CNS/CNT nanocomposites with CNT weight loadings of (a) 16.0%, (b) 25.3%, (c) 34.8%, (d) 42.0% and (e) 47.3% prepared at calcination temperature of 700°C under Ar atmosphere.

Table S3. Composition of the nanocomposites prepared by the one-step molten-salt calcination method.

Catalysts	Co_9S_8 (%)	CNS (%)	CNT (%)
Co_9S_8	100	-	-
Co_9S_8/CNS	48.5	51.5	-
Co_9S_8/CNS/CNT-1	41.2	42.8	16.0
Co_9S_8/CNS/CNT-2	37.6	37.1	25.3
Co_9S_8/CNS/CNT-3	31.1	34.1	34.8
Co_9S_8/CNS/CNT-4	27.8	30.2	42.0
Co_9S_8/CNS/CNT-5	24.6	28.1	47.3

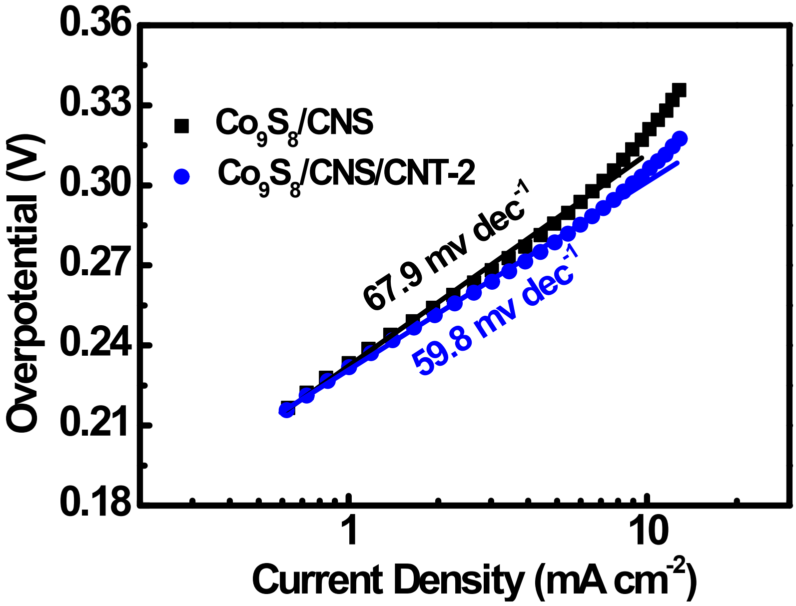

Fig. S14 Tafel plots of Co_9S_8/CNS and Co_9S_8/CNS/CNT-2 catalysts in 0.1 M KOH electrolyte.

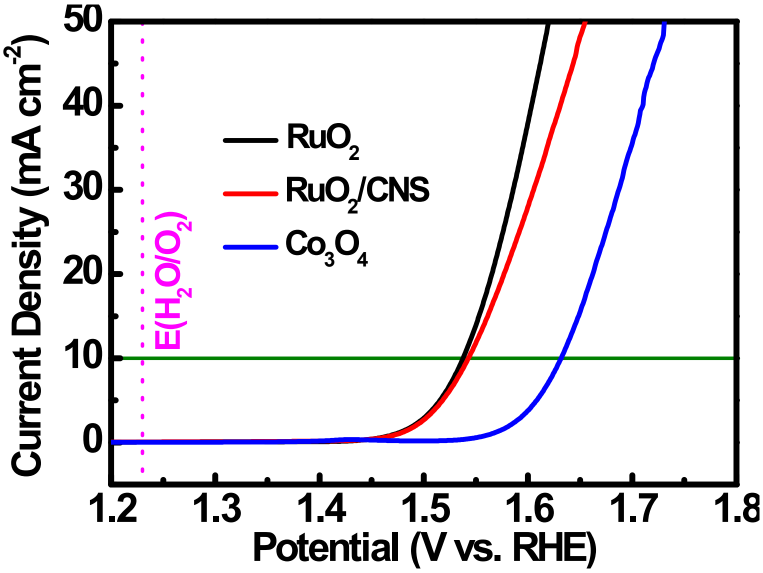

Fig. S15 Polarisation curves of RuO_2, RuO_2/CNS and Co_3O_4 electrocatalysts measured at a scan rate of 5 mV s^{-1} in 1.0 M KOH electrolyte.

To realise the effect of CNS on the OER performance, 48.5% (wt%) of RuO_2 (same weight percentage of Co_9S_8 in Co_9S_8/CNS composite) was mixed with CNS to prepare a composite electrocatalyst and the polarisation curves were measured. As evident from Fig. S15, no significant change in the onset potential was observed. However, a slight decrease in the current density was encountered that possibly due to the difference in chemical property of separately prepared CNS compared to that of the *in situ* grown CNS in Co_9S_8/CNS nanocomposites. Also, cobalt oxide (Co_3O_4) nanopowders with the particle size <50 nm (Sigma-Aldrich, ≥99.5%) as an electrocatalyst for OER was tested in 1.0 M KOH under the same experimental condition used for other samples presented in this work. The polarisation curve obtained for Co_3O_4 indicates a largely anodic shifted onset potential of ~1.55 V (vs. RHE) compare to that of RuO_2. The obtained OER properties of Co_3O_4 are also well aligned with the reported results.[23-25]

Supporting References

1. L. L. Feng, G. D. Li, Y. Liu, Y. Wu, H. Chen, Y. Wang, Y. C. Zou, D. Wang and X. Zou, *ACS Appl. Mater. Interfaces*, 2015, **7**, 980.
2. J. Wang, H. X. Zhong, Z. L. Wang, F. L. Meng and X. B. Zhang, *ACS Nano*, 2016, **10**, 2342.
3. X. Xu, P. Du, Z. Chen and M. Huang, *J. Mater. Chem. A*, 2016, **4**, 10933.
4. W. Fang, D. Liu, Q. Lu, X. Sun and A. M. Asiri, *Electrochem. Commun.*, 2016, **63**, 60.
5. J. Yang, G. Zhu, Y. Liu, J. Xia, Z. Ji, X. Shen and S. Wu, *Adv. Funct. Mat.*, 2016, **26**, 4712.
6. B. K. Barman and K. K. Nanda, *Dalton Trans.*, 2016, **45**, 6352.
7. C. Xia, Q. Jiang, C. Zhao, M. N. Hedhili and H. N. Alshareef, *Adv. Mater.*, 2016, **28**, 77.
8. Y. Liang, Q. Liu, Y. Luo, X. Sun, Y. He and A. M. Asiri, *Electrochem. Commun.*, 2016, **190**, 360.
9. T. Liu, Y. Liang, Q. Liu, X. Sun, Y. He and A. M. Asiri, *Electrochem. Commun.*, 2015, **60**, 92.
10. M. Shen, C. Ruan, Y. Chen, C. Jiang, K. Ai and L. Lu, *ACS Appl. Mater. Interfaces*, 2015, **7**, 1207.
11. H. Zhu, J. Zhang, R. Yanzhang, M. Du, Q. Wang, G. Gao, J. Wu, G. Wu, M. Zhang, B. Liu, J. Yao and X. Zhang, *Adv. Mater.*, 2015, **27**, 4752.
12. I. H. Kwak, H. S. Im, D. M. Jang, Y. W. Kim, K. Park, Y. R. Lim, E. H. Cha and J. Park, *ACS Appl. Mater. Interfaces*, 2016, **8**, 5327.

13. X. Cao, X. Zheng, J. Tian, C. Jin, K. Ke and R. Yang, *Electrochim. Acta*, 2016, **191**, 776.
14. Y. Xu, Y. Hao, G. Zhang, X. Jin, L. Wang, Z. Lu and X. Sun, *Part. Part. Syst. Charact.*, 2016, **33**, 569.
15. W. Zhao, C. Zhang, F. Geng, S. Zhuo and B. Zhang, *ACS Nano*, 2014, **8**, 10909.
16. M. R. Gao, X. Cao, Q. Gao, Y. F. Xu, Y. R. Zheng, J. Jiang and S. H. Yu, *ACS Nano*, 2014, **8**, 3970.
17. P. Ganesan, M. Prabu, J. Sanetuntikul and S. Shanmugam, *ACS Catal.*, 2015, **5**, 3625.
18. S. Dou, L. Tao, J. Huo, S. Wang and L. Dai, *Energy Environ. Sci.*, 2016, **9**, 1320.
19. M. R. Gao, Y. F. Xu, J. Jiang, Y. R. Zheng and S. H. Yu, *J. Am. Chem. Soc.*, 2012, **134**, 2930.
20. H. Wang, Z. Li, G. Li, F. Peng and H. Yu, *Catal. Today*, 2015, **245**, 74.
21. Q. Liu, J. Jin and J. Zhang, *ACS Appl. Mater. Interfaces*, 2013, **5**, 5002.
22. B. Chen, R. Li, G. Ma, X. Gou, Y. Zhu and Y. Xia, *Nanoscale*, 2015, **7**, 20674.
23. X. Li, Y. Fang, X. Lin, M. Tian, X. An, Y. Fu, R. Li, J. Jin and J. Ma, *J. Mater. Chem. A*, 2015, **3**, 17392.
24. Y. X. Zhang, X. Guo, X. Zhai, Y. M. Yan and K. N. Sun, *J. Mater. Chem. A*, 2015, **3**, 1761.
25. M. Q. Yu, L. X. Jiang and H. G. Yang, *Chem. Commun.*, 2015, **51**, 14361.